ENVIRONMENTAL STUDIES

# Loss of geomorphic diversity in shallow tidal embayments promoted by storm-surge barriers

**Davide Tognin[1,2]*†, Alvise Finotello[2,3]*†, Andrea D'Alpaos[2,4], Daniele P. Viero[1], Mattia Pivato[2], Riccardo A. Mel[5], Andrea Defina[1,2], Enrico Bertuzzo[3], Marco Marani[1,2], Luca Carniello[1,2]**



**Coastal flooding prevention measures, such as storm-surge barriers, are being widely adopted globally because of the accelerating rise in sea levels. However, their impacts on the morphodynamics of shallow tidal embayments remain poorly understood. Here, we combine field data and modeling results from the microtidal Venice Lagoon (Italy) to identify short- and long-term consequences of flood regulation on lagoonal landforms. Artificial reduction of water levels enhances wave-induced sediment resuspension from tidal flats, promoting in-channel deposition, at the expense of salt marsh vertical accretion. In Venice, we estimate that the first 15 closures of the recently installed mobile floodgates operated between October 2020 and January 2021 contributed to a 12% reduction in marsh deposition, simultaneously promoting a generalized channel infilling. Therefore, suitable countermeasures need to be taken to offset these processes and prevent significant losses of geomorphic diversity due to repeated floodgate closures, whose frequency will increase as sea levels rise further.**

## INTRODUCTION

Low-lying coastal areas worldwide are threatened by the adverse consequences of flooding hazards related to climate change and rising sea levels (*1*–*4*). To mitigate flooding risk, many coastal cities supporting large populations and economies have adopted hard protection measures in the form of storm-surge barriers (*5*, *6*). Relevant examples are the barriers built to protect The Netherlands, the cities of London and Hull in the United Kingdom, St. Petersburg in Russia, New Orleans in Louisiana, and Venice in Italy. Surge barriers are also being proposed to protect Shanghai and New York, as well as the Galveston Bay in the United States.

Despite the rapidly increasing number of structures to defend coastal cities, the effects of flood regulation measures on the morphodynamic evolution of the tidal areas surrounding them still need to be fully understood (*7*, *8*). Storm-surge barriers may deeply affect the chief coastal land-forming processes, such as tides, surges, and waves (*9*–*11*), affecting sediment transport and the possible survival of many important transitional coastal environments (*12*). This is especially critical in sediment supply–limited, shallow embayments (*13*), where morphodynamics is intimately related to wind-driven sediment resuspension and transport mechanisms and can be deeply affected by changes in water levels because of storm-surge barrier operations.

The Venice Lagoon, Italy, is one of the first examples of a sediment-starved, shallow back-barrier system protected by storm-surge barriers. The set of barriers, known as the Mo.S.E. system (the Italian acronym for Experimental Electromechanical Module), span the three inlets—Lido, Malamocco, and Chioggia from north to south—that connect the Venice Lagoon to the Adriatic Sea (Fig. 1). The mobile barriers are closed to avoid the flooding of Venice when the water level is predicted to exceed 1.10 m above the local reference datum of Punta della Salute (ZPS) (*14*) (corresponding to about 0.79 m above the current mean sea level). Each barrier is made by a series of flapgates (78 in total; Fig. 1), which are hinged along a common horizontal axis and rest flush with the seabed under normal tidal levels to allow for the exchange of water and sediment fluxes, as well as regular ship traffic.

The construction of the Mo.S.E. system began in 2003, and the mobile floodgates were operated for the first time in October 2020, holding back high-tide waters outside the lagoon for the first time in history. Despite the heated public, technical, and scientific debate that has surrounded the Mo.S.E. since its conception in the 1970s (*15*, *16*), the impacts that repeated closures of the lagoon inlets might have on the fate of the characteristic lagoonal landforms—i.e., salt marshes, tidal flats, and tidal channels (Fig. 1A)—have not yet received the necessary attention. These landforms constitute the morphological backbone on which all the relevant morphodynamic and ecological processes rely. For instance, tide propagation and water residence time within the lagoon depend on the morphology of the tidal channel network as well as on the relative extent and bed elevation of tidal flat and salt marsh areas (*17*). Salt marshes are also effective in limiting wind fetch, thereby reducing both wind-wave height and wind setup (*18*–*21*), with direct effects on water levels within the lagoon (*22*). In addition, the morphological structure of the lagoon plays a key role in regulating the exchange of sediments, nutrients, and pollutants with the open sea and provides diverse habitats for many plant and animal species, which are also important for local economies (*23*–*26*).

While there is no doubt that temporarily disconnecting the lagoon from the sea is key to preventing the flooding of Venice and other urban areas during severe storm-surge events (*27*), it is essential to fully understand the potentially cascading effects that repeated inlet closures might have on long-term lagoon morphodynamics. This becomes increasingly critical in view of the rise in the mean sea level expected over the next century (*1*, *2*, *4*), which will inevitably lead to more frequent closures (*28*).

Here, we use field data and numerical modeling of barrier activations from October 2020 to January 2021, focusing particularly

[1]University of Padova, Department of Civil, Environmental, and Architectural Engineering, IT-35131 Padova, Italy. [2]University of Padova, Center for Lagoon Hydrodynamics and Morphodynamics (C.I.Mo.La.), IT-35131 Padova, Italy. [3]Ca' Foscari University of Venice, Department of Environmental Sciences, Informatics and Statistics, IT-30172 Mestre, Venice, Italy. [4]University of Padova, Department of Geosciences, Padova, IT-35131 Padova, Italy. [5]University of Calabria, Department of Environmental Engineering, IT-87036 Cosenza, Italy.
*Corresponding author. Email: davide.tognin@phd.unipd.it (D.T.); alvise.finotello@unive.it (A.F.)
†These authors contributed equally to this work.

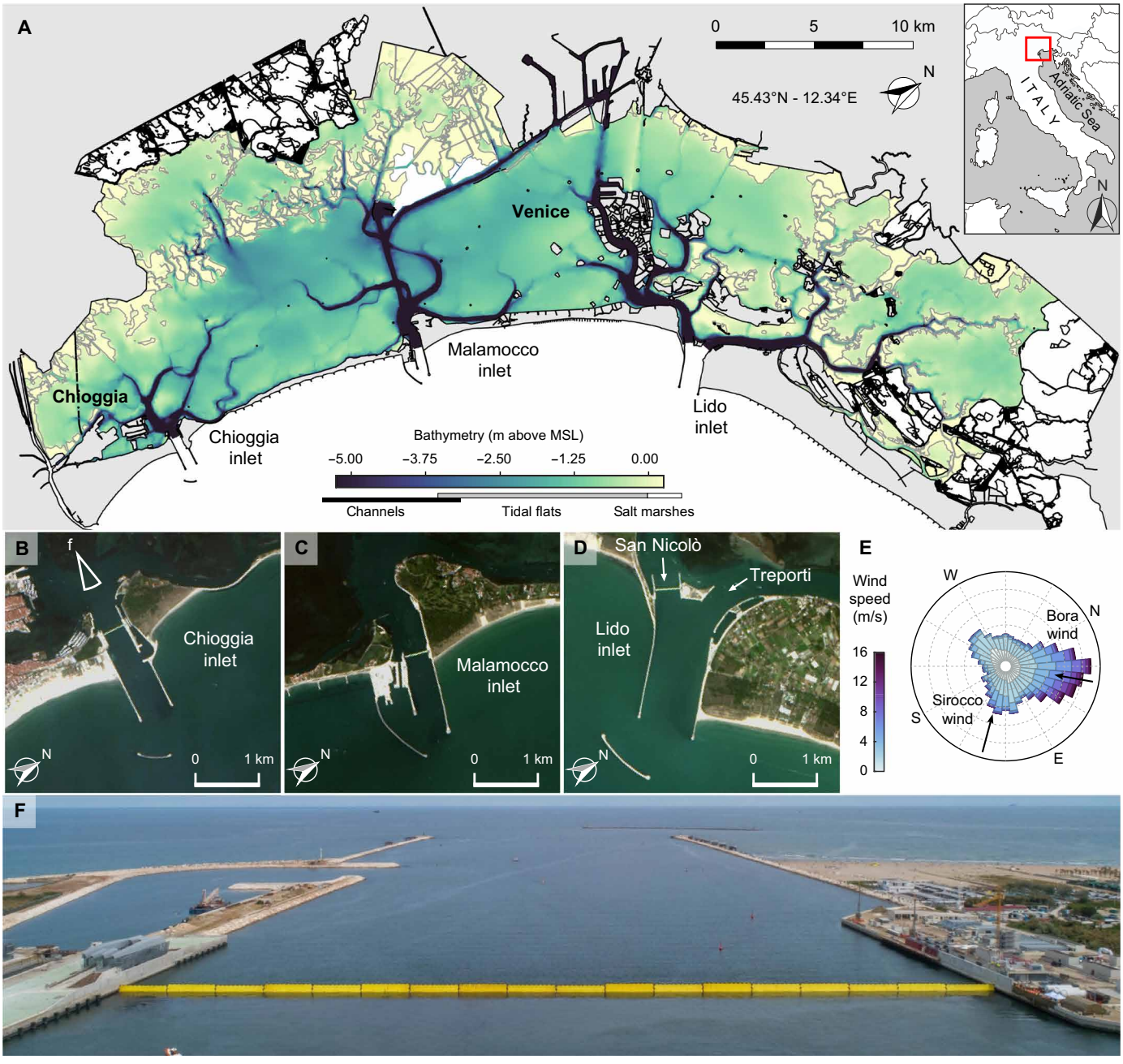


**Fig. 1. Geomorphological setting and floodgates.** (**A**) Bathymetry of the Venice Lagoon located in northeastern Italy (inset). MSL, mean sea level. Salt marshes are indicated by the gray contour. Chioggia inlet (360 m wide, 12 m deep, 18 gates) (**B**), Malamocco inlet (380 m wide, 14 m deep, 19 gates) (**C**), and Lido inlet (**D**), divided into the San Nicolò barrier (400 m wide, 12 m deep, 20 gates) and the Treporti barrier (420 m wide, 6 m deep, 21 gates; still submerged during the test in the satellite image), during the closure test on 9 October 2020, 10:00 UTC (Landsat 8 NASA). (**E**) Wind rose for the period 2000–2019 measured in Chioggia; arrows highlight the two morphologically significant winds [Bora, northeast (NE); Sirocco, southeast (SE)]. (**F**) The Mo.S.E. barrier during a closure at the Chioggia inlet [photo position indicated in (B); photo credits: www.mosevenezia.eu/].

on the first two closures that occurred on 3 and 15 October 2020, to understand the impacts of flood regulation on sediment transport within the lagoon and their possible implications for the morphological evolution of lagoonal landforms. We adopted a custom-built, extensively tested two-dimensional (2D) finite-element numerical model able to reproduce morphodynamic processes within the Venice Lagoon (*14*, *29*, *30*) (see Materials and Methods). To better understand the effects of the Mo.S.E. operations, the results for the flood-regulated scenario are compared with those for nonregulated conditions, which would have occurred in the absence of the floodgate closures. Results of the simulations are then analyzed in terms of differences in water levels, bottom shear stresses, suspended sediment concentrations (SSCs), and salt marsh flooding. Long-term effects of floodgate closures on the morphodynamics of the whole

lagoon, as well as potential cascading effects due to the degradation of lagoonal landforms, are finally discussed together with possible mitigation solutions.

## RESULTS

### Effects on the lagoon hydrodynamics

The Mo.S.E. floodgates were raised to hold water levels within the lagoon below the safety threshold of 1.10 m above the local datum (ZPS), for both the storm-surge events of 3 and 15 October 2020 (Fig. 2 and figs. S2 and S3). Maximum measured water levels in the lagoon reached 0.80 ± 0.03 m (mean ± SD) above ZPS during the storm-surge event of 3 October, characterized by a mild southeasterly Sirocco breeze (average and maximum wind speeds $v_{avg}$ = 8.1 m/s and $v_{max}$ = 13.7 m/s, respectively; Fig. 2A and fig. S8A) and a reduced wind setup equal to $\delta^{+}_{W_{avg}}$ = 0.08 m between the western and eastern parts of the lagoon (Fig. 2, A and C, and fig. S8A). In contrast, on 15 October, although the maximum measured water levels in the lagoon were limited to 0.69 ± 0.17 m above ZPS, the strong northeasterly Bora wind ($v_{avg}$ = 14.8 m/s and $v_{max}$ = 22.8 m/s) blowing along the main axis of the lagoon generated a pronounced water setup, with an average difference in the maximum observed water levels between the northern and southern parts of the lagoon equal to $\delta^{+}_{W_{avg}}$ = 0.45 m (Fig. 2, B and D, and fig. S8B).

Model results, which accurately reproduce observed water levels (mean absolute error, 0.016 to 0.043 m; Nash-Sutcliffe efficiency, 0.94 to 0.99; figs. S2 and S3 and table S1), indicate that water level reduction with respect to the levels that would have occurred in the absence of the gate closure was not uniform within the lagoon (Fig. 2, C and D, and fig. S8). In particular, for the 3 October event, the reduction in maximum water levels was less pronounced in the northern lagoon (0.36 ± 0.05 m, 38%), where the interplay between naturally preserved shallow tidal flats, deeply incised channels, and widespread salt marshes promotes natural damping of the tidal wave also when the floodgates are open. On the contrary, a larger water level reduction, as high as 0.46 ± 0.03 m (45%), was observed in the central and southern parts of the lagoon, as well as in the proximity of Venice. This is mainly dictated by the less significant dissipation of the tidal wave in these portions of the lagoon (*31*), where marsh areas are less widespread and tidal flats are deeper (*32*). In the case of the strong Bora wind, as for the 15 October event, the largest water level reduction relative to the nonregulated scenario was again observed in the central lagoon (0.69 ± 0.04 m, 57%). Although the northern and southern portions show the same value of the absolute reduction

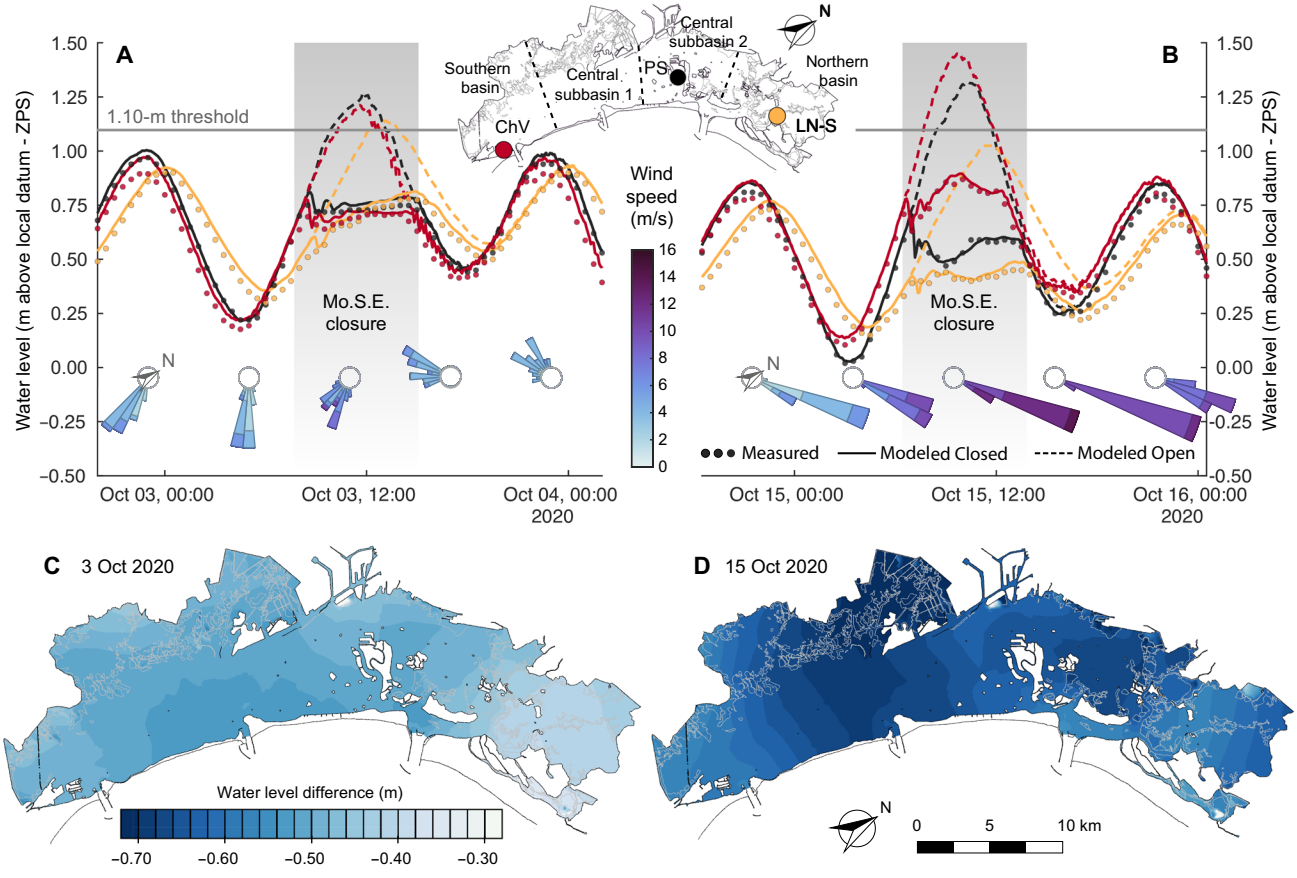


**Fig. 2. Effect of floodgate closure on the lagoon hydrodynamics.** Water level and wind conditions for the 3 October (**A**) and 15 October 2020 (**B**) events. Solid circles represent water level measurements in three different stations [Punta della Salute (PS), Laguna Nord–Saline (LN-S), and Chioggia Vigo (ChV)] represented in the inset, and solid and dashed lines represent water levels modeled in closed and open barrier scenarios, respectively. Wind roses show wind conditions grouped by 6-hour-long intervals and measured in the Laguna Nord–Saline station. Gray background indicates the time span of Mo.S.E. closures. Difference between maximum modeled water level in the closed and open barrier scenarios for the 3 October (**C**) and 15 October 2020 (**D**) events.

(0.59 ± 0.05 m), the relative impact is different in the two cases. This absolute reduction represents a relative water level attenuation of 71% in the northern part, where the water level would have been relatively low even with open inlets, because of the enhanced wind setup pushing the water in the southeastern direction. In contrast, the relative water level attenuation in the southern basin, where stormwater levels would have been comparatively higher in the absence of flood regulation, is about 46%.

### Effects on tidal flat and channel morphodynamics

Hydrodynamic changes due to the Mo.S.E. operations can appreciably affect sediment transport in the lower-intertidal and subtidal zones by modifying the local bottom shear stress ($\tau_b$ ) (*33*, *34*), which is primarily responsible for sediment resuspension.

On tidal flats, reduced water levels due to the closure of the inlets increase bottom friction and favor wave breaking. Model simulations of the open and closed scenario show that, as a result of this process, the maximum significant wave height ($H_s$) was reduced by 8% (mean reduction, 0.02 m; maximum, 0.23 m) on 3 October, and by 20% (mean reduction, 0.10 m; maximum, 0.45 m) on 15 October (Fig. 3, A and B, and fig. S9). Although wave height is reduced, shallower water depths imposed by barrier closures determine larger values of $\tau_b$ across tidal flat areas (*33*). Hence, the overall result of the reduced water levels during inlet closures is an increase in the maximum value of $\tau_b$ of about 5% (mean increase, 0.02 Pa; maximum, 0.21 Pa) for the 3 October event and of 20% (mean increase, 0.10 Pa; maximum, 0.52 Pa) for the 15 October event (Fig. 3, C and D, and fig. S10). In contrast, $\tau_b$ tends to decrease within the main channels close to the inlets, where the

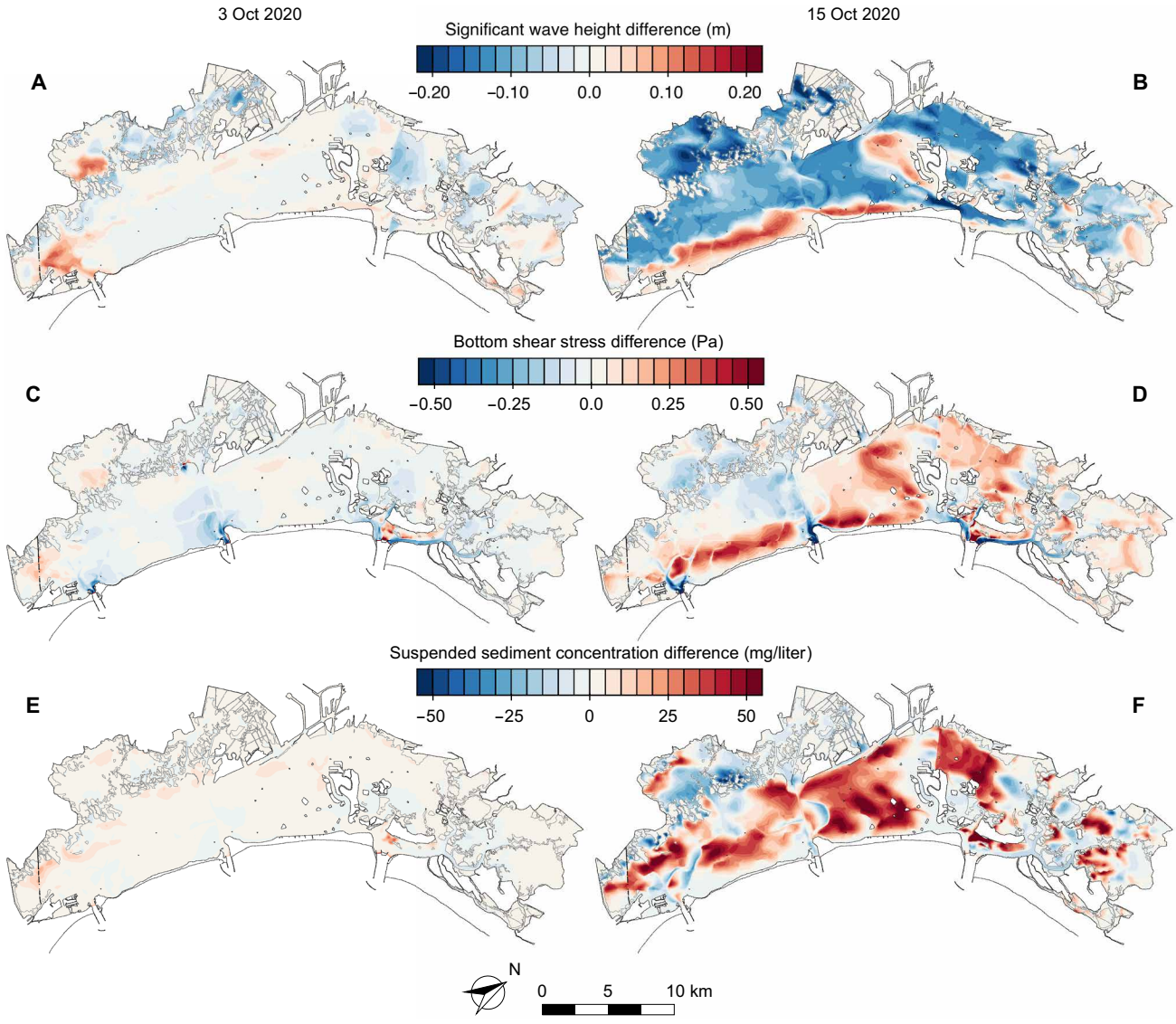


**Fig. 3. Effect of floodgate closure on sediment resuspension within tidal flats and channels.** Difference between maximum modeled significant wave height in the closed and open barrier scenarios for the 3 October (**A**) and 15 October 2020 (**B**) events. Difference between maximum modeled bottom shear stress in the closed and open barrier scenarios for the 3 October (**C**) and 15 October 2020 (**D**) events. Difference between maximum modeled SSC in the closed and open barrier scenarios for the 3 October (**E**) and 15 October 2020 (**F**) events. All these maps were obtained by subtracting, for each of the parameters of interest, the maximum values observed in the closed and open barrier scenarios over the whole simulation horizon. Salt marshes are highlighted by gray lines.

tidal currents, and hence the associated bed shear stresses, are largely reduced because of the gate closures (Fig. 3, C and D).

During both closure events, the increase in $\tau_b$ over tidal flats leads to a generalized increase in the SSC. Measured SSC shows peaks of 120 mg liter$^{-1}$ during the closures (fig. S4). Modeled SSC, although not as closely as in the case of water levels, reasonably matches measurements, reproducing the magnitude and the modulation induced by tidal levels and wind waves (mean absolute error, 1.16–8.91 mg liter$^{-1}$; Nash-Sutcliffe efficiency, 0.49 to 0.64; table S2). On 3 October, maximum modeled SSC was, on average, 4.5% higher than in the open lagoon scenario (mean increase, 4.4 mg liter$^{-1}$; maximum, 20.3 mg liter$^{-1}$; Fig. 3E). In contrast, much higher wind speeds and, hence, $\tau_b$ resulted in an average increase in the SSC maxima of 21% (mean increase, 25.4 mg liter$^{-1}$; maximum, 71.6 mg liter$^{-1}$) on 15 October, with extensive areas experiencing increments well above 50 mg liter$^{-1}$ (Fig. 3F and fig. S11).

Therefore, floodgate closures can significantly enhance the amount of sediment resuspended from the lagoon bed, especially if combined with strong winds that typically occur during storm-surge events (*35*). This circumstance might be further exacerbated by the fact that barrier closures are more likely in the late fall and winter when the biomass of both seagrass and benthic biofilm is reduced because of seasonal dynamics, thus offering relatively little protection against sediment erosion of the lagoon bottom (*36*, *37*).

### Effects on salt marsh morphodynamics

Changes in the hydrodynamic circulation and sediment dynamics due to inlet closures also have important effects on the evolution of salt marshes, which occupy the upper intertidal frame. First, by limiting high tides and storm surges, Mo.S.E. operations significantly reduce both the intensity and duration of salt marsh flooding (Fig. 4 and figs. S12 and S13). On 3 October 2020, the above-marsh water depth was reduced by 0.42 ± 0.05 m (64%; maximum value, 0.52 m; Fig. 4A), and the flooding duration was reduced by 1.4 hours (30%) on average, with a maximum reduction of 6.3 hours (Fig. 4C). Although salt marsh areas in the central and southern lagoon suffered slightly more pronounced reductions, the above changes were approximately uniform in space during this event. In contrast, the stronger winds on 15 October pushed large amounts of water toward the southern end of the lagoon, and almost half of the total salt marsh area (46.5%) remained dry as a result, especially in the northern lagoon (Fig. 4D). Numerical simulations suggest that all these marshes would have been otherwise flooded in the open lagoon scenario (fig. S12). The closure determined an average reduction in flooding depth of about 0.63 ± 0.07 m (73%; maximum, 0.98 m; Fig. 4B), while the flooding duration decreased by 2.8 hours (55%) on average (maximum value, 7.28 hours; Fig. 4D).

The reduction in marsh flooding duration and depth caused by gate closures has important implications, as periodic flooding is the only mechanism through which the suspended sediment carried by high waters can reach the marsh surface and contribute (together with organic sediment production by vegetation) to salt marsh vertical accretion and to their ability to keep up with sea level rise (*38*–*41*). While daily tidal inundations can only marginally contribute to salt marsh vertical accretion, because of the reduced flooding duration and low SSC, surge-induced marsh flooding is typically in phase with peaks of SSC caused by intense wind-wave resuspension from tidal flats (*36*), and it is characterized by larger water depths and longer

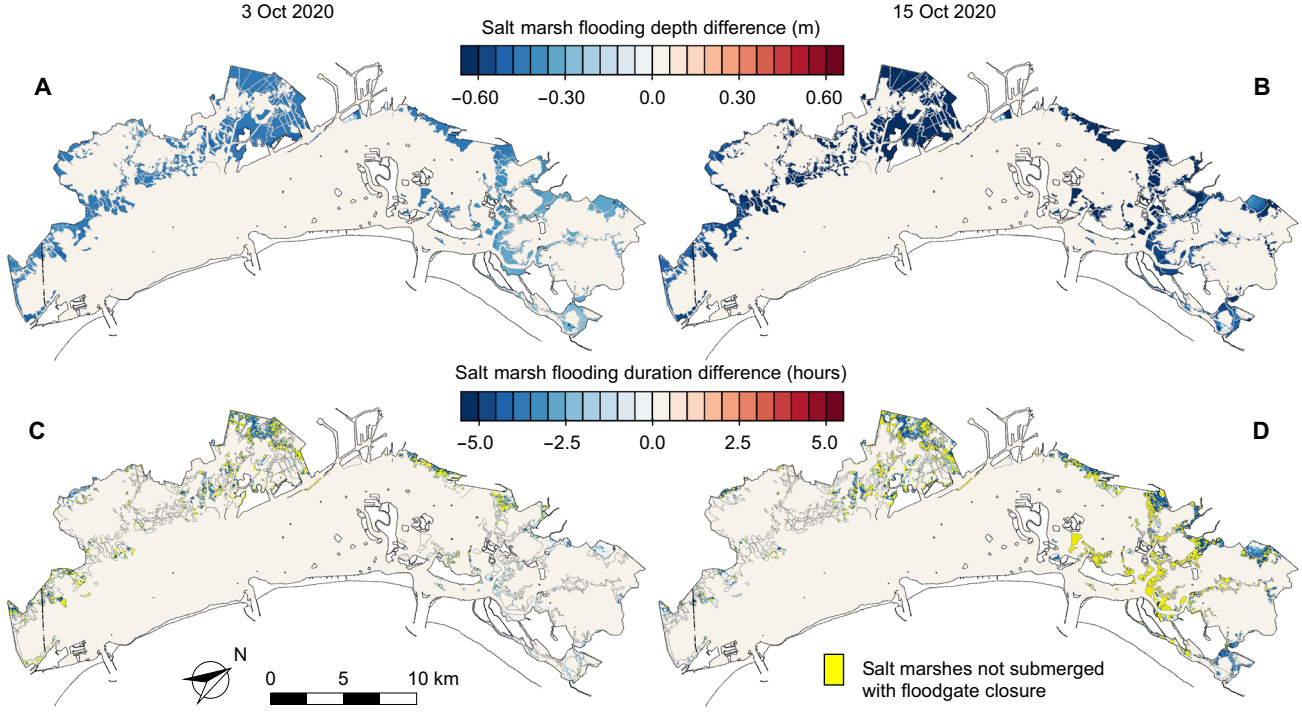


**Fig. 4. Effect of floodgate closure on salt marsh flooding.** Difference between maximum modeled salt marsh flooding depth in the closed and open barrier scenario for the 3 October (**A**) and 15 October 2020 (**B**) events. Difference between maximum salt marsh flooding duration in the closed and open barrier scenario for the 3 October (**C**) and 15 October 2020 (**D**) events. All these maps were obtained by subtracting, for each of the parameters of interest, the maximum values observed in the closed and open barrier scenarios over the whole simulation horizon. Salt marshes are highlighted by gray lines.

durations, thus ultimately contributing to the deposition of larger sediment volumes (*42*). Recent field measurements of marsh sedimentation suggest that, although limited in time, flooding reduction related to floodgate closures critically influences the sustainability of salt marshes (*42*).

In contrast, floodgate closures only marginally affect marsh lateral erosion. Although the power of wind waves per unit length of marsh margin can change because of wave height and water-level modifications, these variations are typically smaller than 5% (absolute values of 0.01 ± 0.36 W/m for the 3 October event and 0.21 ± 1.38 W/m for the 15 October event; fig. S14). Given the functional linear relationship between incoming mean wave power and marsh edge retreat rates (*43*, *44*), these changes are not likely to produce significant modifications in the rates at which marsh margins within the Venice Lagoon are currently being eroded (*20*).

## Sediment budget at the basin scale

The primary effect of water-level reduction caused by inlet closures is to enhance sediment resuspension. In general, the fate of suspended sediments can be manifold, as they may settle on tidal flats, accumulate over salt marshes when these are flooded, deposit within the channels, or may be transported through the channel network and the inlets to the open sea. To quantify each of these sediment fluxes, we track the temporal evolution of eroded and deposited sediment volumes for each of the different morphological units in each closure event (Fig. 5, A to D). We also quantify

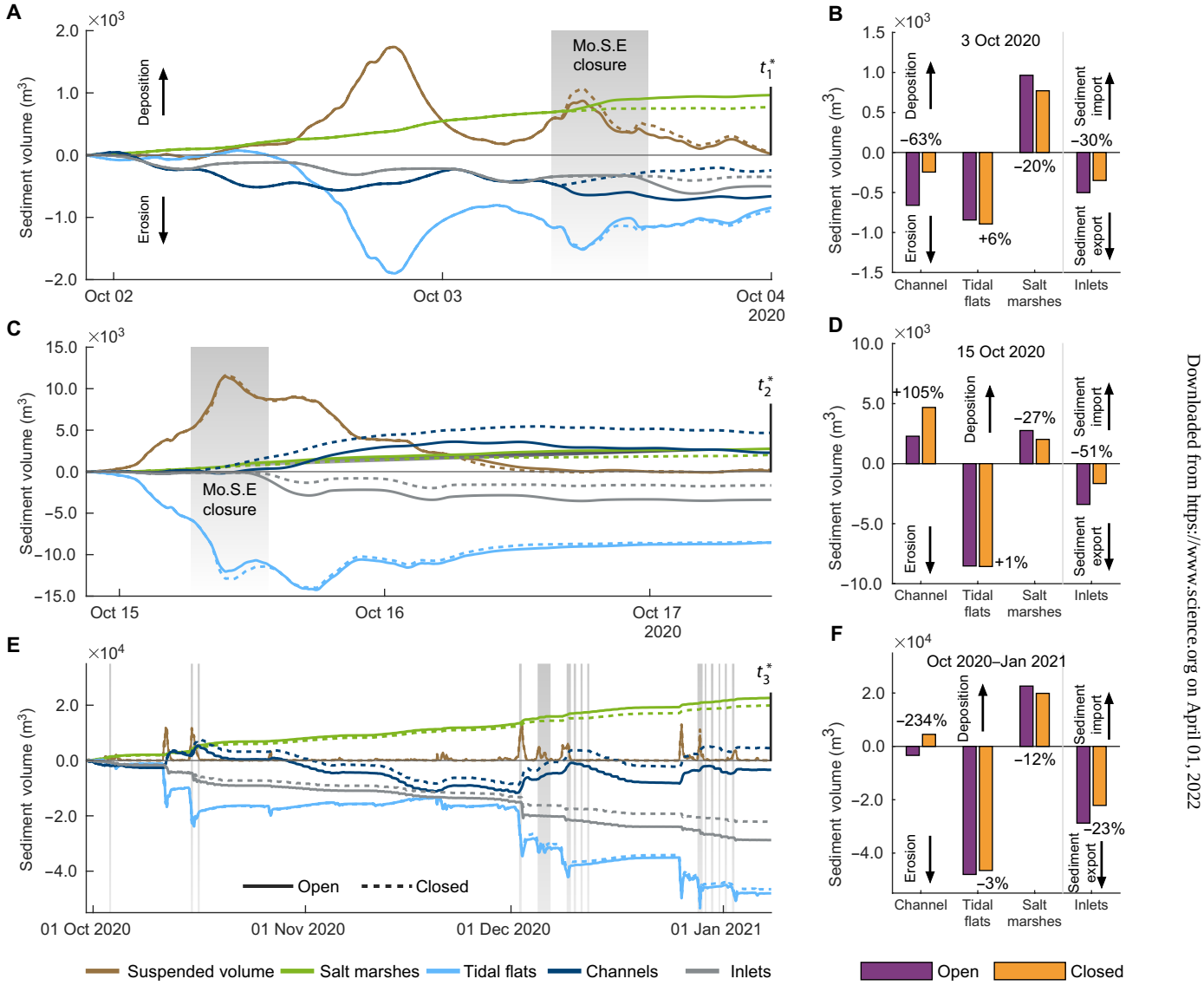


**Fig. 5. Effect of floodgates closure on the sediment budget.** Sediment volume changes through time for different morphological units (salt marshes, tidal flats, and channels), suspended sediment, and import/export through inlets for the 3 October event (**A**), the 15 October event (**C**), and the period October 2020–January 2021 (**E**). Continuous lines refer to the open barrier scenario, and dashed lines refer to the closed barrier one. Gray background indicates the time span of Mo.S.E. closures. Net sediment volume changes at the end of the events, when suspended sediment volume returns negligible (**B**, **D**, and **F**). The time instants *t** considered for the net volume change represented are indicated in (A), (C), and (E). Percentages indicated the relative change in the closed barrier scenario with respect to the open barrier one.

sediment budget changes on a longer time scale, accounting for all the 15 floodgate closures that occurred between October 2020 and January 2021 (Fig. 5, E and F).

Sediment export to the open sea is temporarily reduced by the floodgate closures by 30% (151 $m^3$) on 3 October and by 51% (1740 $m^3$) on 15 October. Overall, we estimate that the Mo.S.E. closures have led to a 23% reduction (6630 $m^3$) in net sediment export (gray lines, Fig. 5, A, C, and E) during the period October 2020–January 2021. Floodgate closures only slightly increased erosion of tidal flats by +6% (49 $m^3$) and + 1% (45 $m^3$) on 3 and 15 October, respectively (Fig. 5, B and D), although such erosion levels out at seasonal time scale (Fig. 5F). Sediments reworked from tidal flats during closures are partially advected elsewhere by wind-induced secondary circulation and partially settle within the channel network, reducing channel erosion by 63% (415 $m^3$) on 3 October or increasing channel infilling by 105% (2399 $m^3$) on 15 October compared to the open lagoon scenario. On a seasonal time scale, repeated floodgate closures ultimately promote channel infilling through the deposition of sediment resuspended from tidal flats (Fig. 5F). In contrast, water-level reduction due to inlet closures contributes to a substantial reduction of sediment volumes delivered to salt marsh areas. This reduction equals 20% (193 $m^3$) for the 3 October event and 27% (737 $m^3$) for the 15 October event (Fig. 5, B and D) and occurs because of reduced flooding depths and durations (Fig. 4), despite SSC being much higher than in the nonregulated scenario (Fig. 3, E and F). On a seasonal time scale, model estimates indicate a reduction of the volume deposited on salt marsh surfaces of about 12% (2760 $m^3$) due to the 15 floodgate closures in October 2020–January 2021.

To better understand the mechanisms that lead to reduced sedimentation on the marshes, the fate of sediment resuspended from the lagoon bottom is analyzed using a visualization technique based on Lagrangian particle tracking (see Materials and Methods). As an example, we have followed the paths of resuspended sediments in two different areas of the lagoon during the barrier operations of both 3 and 15 October and compared them with the corresponding trajectories obtained by keeping the lagoon open to tidal fluxes (Fig. 6). In the open lagoon scenario, the amount of resuspended sediment that reaches the marsh surface and settles therein is relevant, although variable in space depending on the directions of both tidal currents and wind waves (Fig. 6). Specifically, on 3 October, about 20% of the sediment particles resuspended from the analyzed tidal flats would have settled over the adjacent salt marshes in the open lagoon scenario (purple dots, Fig. 6, A and C), while on 15 October, higher water levels and stronger winds would have further enhanced sediment settling up to 53%, especially on salt marshes located in the southern lagoon and exposed directly to the incoming Bora winds (purple dots, Fig. 6D). The same wind setup strongly limits sedimentation over the marshes in the northern lagoon because of the local reduction in the water level (purple dots, Fig. 6B). Conversely, when the Mo.S.E. is activated, sediments remain confined within tidal channels and over tidal flat areas because of reduced water levels and are not advected over marshes, where particle deposition is reduced by 30 to 100% compared with the nonregulated scenario (yellow dots, Fig. 6). This effect can only be partially mitigated by the local wind setup. For instance, during the event of 15 October, water setup generated by the northeasterly gale allowed for active sediment delivery to southern lagoon marshes, although the total amount of deposited sediment particles was halved compared with the open lagoon scenario (Fig. 6D).

## DISCUSSION

The temporary closure of a shallow tidal basin aimed at preventing urban flooding can deeply affect its morphodynamics and poses a major threat to tidal wetland sustainability, particularly under accelerating sea level rise. Repeated floodgate closures promote sediment reworking on tidal flats and channel infilling while hindering salt marsh vertical accretion. The increased sediment retention caused by floodgate closures promotes a less-diverse geomorphological structure, rather than contributing to the preservation of tidal landforms.

Overall, when floodgates are operated, channels tend to be infilled by the increased resuspension on tidal flats, reduced sediment delivery to marshes, and the additional volume of sediment retained within the basin. However, the pattern of channel bed evolution depends on both the temporal scale considered and the local morphodynamic. In channel networks dissecting the inner portions of the lagoon, sediments can hardly be remobilized by weak tidal currents. The deposited sediments thus actively contribute to permanent channel infill and increase dredging costs to maintain the navigability of waterways. Conversely, within the major channels and closer to the inlets, sediments are temporarily accumulated during barrier closures, but, on a longer time scale, they can be remobilized by the higher tidal velocities and eventually will be slowly flushed out to the open sea because of the general ebb-dominated character of tidal currents in the Venice Lagoon (*31*, *45*). Although it might partially counterbalance the increased in-channel deposition, the sediment export induced by ebb currents represents a net loss for the sediment budget at the basin scale. Therefore, both permanent channel infill and sediment export by ebb-dominated tidal currents bear negative implications for the sediment budget and the maintenance of the lagoon geomorphic diversity.

Moreover, artificially lowered water levels reduce the volume of suspended sediment advected over salt marshes, thus depriving them of a critical sediment source. Although floodgate closures can temporarily increase the volume of sediment available in suspension, due to enhanced sediment resuspension from tidal flats, the reduced marsh inundation causes a substantial decrease in the volume of sediment delivered to salt marshes. This mechanism is confirmed by field data, showing that marsh sedimentation increases exponentially with inundation depth (*42*), with water levels capped by floodgate closures determining much lower sediment accumulation. This might ultimately lead to extensive marsh drowning, which, together with the ongoing lateral erosion, will further accelerate the rate at which salt marshes are lost in the Venice Lagoon during the last four centuries (*20*, *32*). Additional salt marsh losses might have critical implications not only from an ecosystem perspective (*25*, *26*), because of the loss in biodiversity and ecosystem services that it would signify, but also for flood-risk mitigation. Further loss of salt marsh surfaces can potentially trigger positive morphodynamic feedbacks (*46*), with detrimental cascading effects for the whole lagoon basin. Decreasing marsh area favors an inertially dominated tidal propagation and increases wind fetch, and thus wave height. Stronger tidal currents and higher wind waves would further exacerbate the ongoing erosive processes within the lagoon, paving the way to the transition from a tidal lagoon to a bay environment (*32*). Moreover, less significant dissipation of tides leads to local increases in the mean high water level (*22*), and larger wind fetches can induce more pronounced water-level setups, in this way potentially offsetting, at least partially, the benefits of flood protection measures.

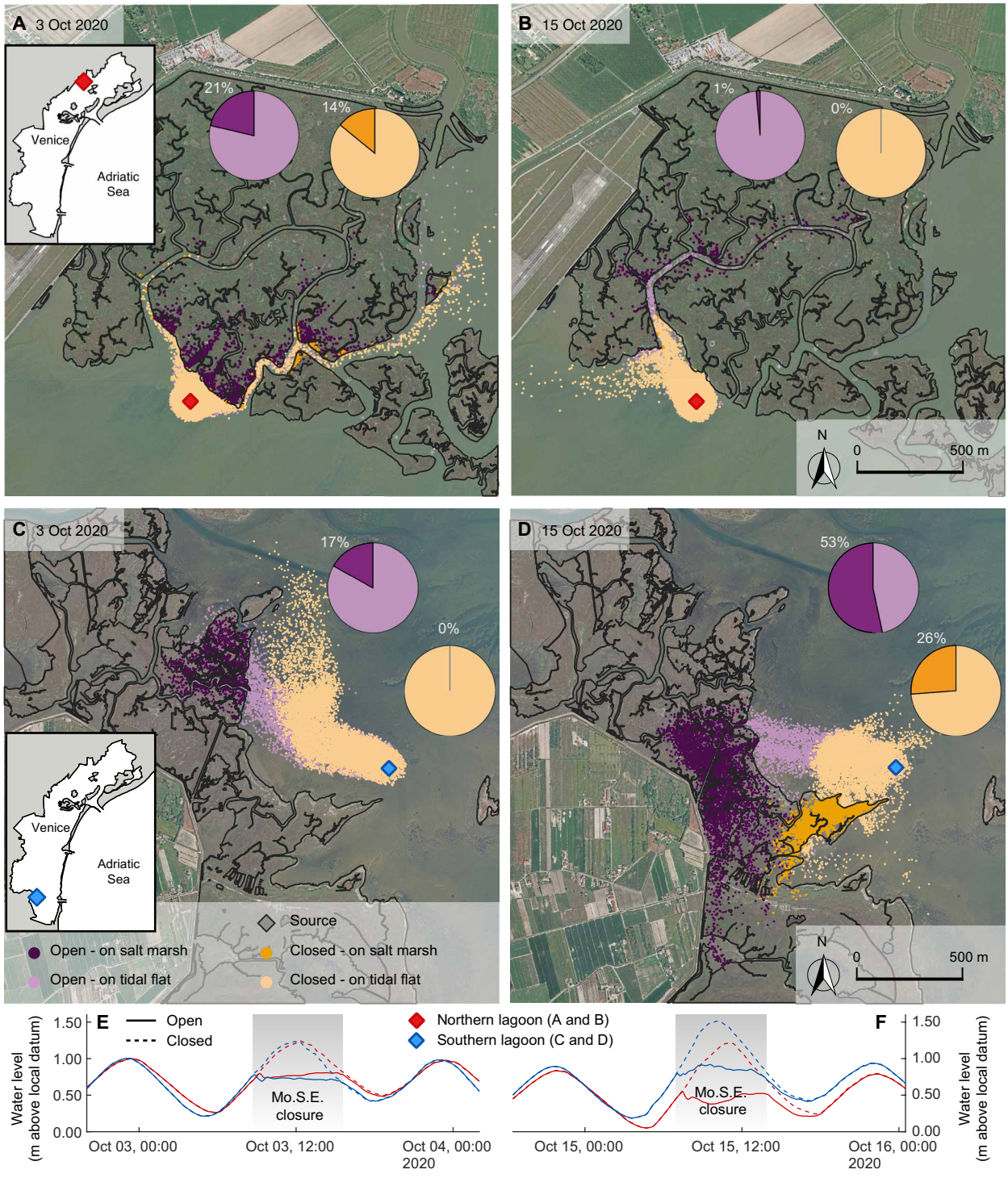


**Fig. 6. Effect of floodgate closure on the suspended sediment fate.** Particle position at the end of the 3 October (**A** and **C**) and 15 October (**B** and **D**) events for two different salt marsh areas, one in the northern lagoon (red diamond) and one in the southern lagoon (blue diamond). A total of 10,000 particles are released at the source point (diamond) at the beginning of the closure in both open and closed barrier scenarios. Pie charts show the percentage of particle that reaches the salt marsh in the scenario with (darker yellow) and without (darker purple) barrier closure. Water levels modeled in front of the two marshes (**E** and **F**).

On the one hand, we emphasize that the effect of flood regulation on the morphodynamics depends exclusively on the reduced water level within the lagoon, and it is not strictly related to the type of floodgates adopted. On the other hand, our analysis suggests that environmental sustainability should have a high priority for designing and managing storm-surge barriers. Trade-offs between the safeguarding of urban areas from flooding and the preservation of tidal ecosystem needs will be essential to ensure adequate resilience against

climate change to shallow tidal embayments where flood barriers operate. In the specific case of the Venice Lagoon, many complementary solutions could be exploited by coastal managers to mitigate the detrimental morphodynamic effects of repeated inlet closures. These solutions, none of which suffice on their own to compensate for the loss of geomorphic diversity, include (i) the artificial raising of sidewalk elevation in the major urban settlements within the lagoon, aimed to increase the current safety water level and reduce the frequency with which floodgates have to be closed; (ii) the reintroduction of fluvial sediment to compensate for the loss of inorganic sediment, both over tidal flats and salt marshes; (iii) the extensive building and restoration of salt marshes, especially adopting nature-based techniques (*47*–*49*); and (iv) the protection of tidal flats and salt marshes against erosion by preserving and improving the ecological conditions that promote the colonization by benthic vegetation, seagrasses, and halophytes, and through the realization of eco-engineering solutions to mitigate sediment erosion, such as oyster reefs and mussel beds (*48*, *50*), able to limit wind fetch, dissipate wave energy, and act as breakwaters for high water levels. These interventions, together with careful management of the floodgate operations and improved weather forecasting tools, would make it possible to ensure flood protection of Venice and other inhabited lagoonal settlements while preserving the lagoon ecosystem as a whole.

## MATERIALS AND METHODS

### Geomorphological setting

The Venice Lagoon, Italy (Fig. 1A), is the largest brackish tidal basin of the Mediterranean Sea, with an area of about 550 km$^2$. It is a shallow microtidal basin, characterized by a semidiurnal tidal regime with an average range of 1.0 m and a mean water depth over the tidal flats of about 1.5 m. It is connected to the Adriatic Sea through three inlets: Lido, Malamocco, and Chioggia from north to south (Fig. 1, B to D). The main morphologically significant winds are represented by the northeasterly Bora wind and the southeasterly Sirocco wind (Fig. 1E). Because of the northeast-southwest elongated shape of the Venice Lagoon, the Bora wind can generate relatively large waves (~ 1 m), especially in the southern sector of the lagoon.

Human interventions have been modifying the Venice Lagoon for centuries. To prevent the lagoon from infilling with fluvial sediment and, therefore, preserve navigability, the Venetian Republic diverted all large rivers to the sea. This process began in 1457 and changed the sediment balance of the basin, triggering sediment starvation and a generalized deepening of the lagoon (*32*). From the end of the 19th century to the mid of the 20th century, sediment export toward the sea was further exacerbated by the construction of the jetties at the inlets (Lido, 1882–1892; Malamocco, 1813–1872; and Chioggia, 1910–1934) (*32*, *45*).

Between 1930 and 1970, intense groundwater exploitation for industrial purposes enhanced loss of relative elevation, resulting in an overall relative sea level rise equal to 25 cm (*51*). Because of subsidence and eustatic sea level rise, the city of Venice started experiencing even more frequent flooding during storm surges. The solution proposed after the catastrophic flooding event of 4 November 1966 (maximum water level of 1.94 m above the local Punta della Salute datum) was the Mo.S.E. project (Fig. 1, B to D and F).

### Hydromorphodynamic model

We adopted a 2D model that consists of three modules, namely, the hydrodynamic module coupled with the wind-wave module (WWTM) (*30*) and the sediment transport and bed evolution module (STABEM) (*29*) suitable for reproducing sediment dynamics governing the morphodynamic evolution of shallow microtidal basins.

The hydrodynamic module solves the 2D depth-integrated shallow water equations (SWEs), phase averaged over a representative elementary area of irregular topography to deal with very shallow flows, wetting, and drying (*52*). Projected on a Cartesian frame ($x$, $y$), the SWEs read

$$\vartheta(\eta)\frac{\partial \eta}{\partial t} + \nabla \cdot \mathbf{q} = 0 \tag{1}$$

$$\frac{D}{Dt}\left(\frac{\mathbf{q}}{Y}\right) + \frac{1}{Y}\nabla \cdot \mathbf{Re} + \frac{\boldsymbol{\tau}_t}{Y\rho} - \frac{\boldsymbol{\tau}_s}{Y\rho} + g\nabla h = 0 \tag{2}$$

where $t$ is time, $\eta$ is is the free surface elevation over a datum, $\mathbf{q} = (q_x, q_y)$ is the depth-integrated velocity (i.e., discharge per unit width), and $\nabla$ and $\nabla\cdot$ denote the 2D gradient and divergence operators. The term $\vartheta$ is the wet fraction of the computational domain that depends on the water depth and on the local topographic unevenness (*52*). In the momentum Eq. 2, $D/Dt$ is the material (or Lagrangian) time derivative; $Y$ is the water volume per unit area (i.e., the equivalent water depth); $\boldsymbol{\tau}_t$ and $\boldsymbol{\tau}_s$ are the shear stresses at the bottom (due to tidal currents) and at the free surface (due to wind drag), respectively; $\rho$ is the water density; and $g$ is gravity. The Reynolds stresses are computed using a depth-averaged version of Smagorinsky's model (*53*). In tensor index notation, they read

$$\mathbf{Re} = R_{ij} = \nu_e Y(u_{i,j} + u_{j,i}) \tag{3}$$

$$\nu_e = 2C_S^2 A_e \sqrt{2(u_{x,x})^2 + (u_{x,y} + u_{y,x})^2 + 2(u_{y,y})^2} \tag{4}$$

with $i$, $j$ in Eq. 3 denoting either the $x$ or $y$ coordinate, and $\mathbf{u} = \mathbf{q}/Y$. The eddy viscosity, $\nu_e$, is proportional to the strain rate, with $A_e$ the area of the computational element and $C_s = 0.2$ the Smagorinsky coefficient.

In the numerical scheme, the material derivative in Eq. 2 is expressed as the finite difference in time and solved with the method of characteristics. This mixed Eulerian-Lagrangian approach allows solving the continuity equation (Eq. 1) with a semi-implicit scheme, which leads to a self-adjoint spatial operator. It is solved on a staggered triangular grid with the finite element method of Galerkin (*52*), and flow rates are obtained by back substitution.

The wind-wave module (*30*) solves the wave action conservation equation using the same computational grid of the hydrodynamic module, which provides water depths and depth-averaged flow velocities, used to propagate the wind-wave field. The wave action density ($N_0$) in the frequency domain evolves according to (*30*)

$$\frac{\partial N_0}{\partial t} + \frac{\partial}{\partial x}c'_{gx}N_0 + \frac{\partial}{\partial y}c'_{gy}N_0 = S_0 \tag{5}$$

where $c'_{gx}$ and $c'_{gy}$ are the group celerity components of wave used to approximate the propagation speed of $N_0$ (*30*, *54*). The wind-wave source terms, grouped in the term $S_0$, account for positive (wind energy input) and negative (bottom friction, whitecapping, and depth-induced breaking) contributions to wave energy. The model computes

the spatial and temporal distribution of the wave periods based on the relationship between peak-wave period, local wind speed, and water depth (*55*). As the lagoon margins are almost vertical and jagged, refraction is neglected and waves are assumed to propagate in the wind direction. The horizontal orbital velocity at the bottom, which is obtained from the significant wave height through the linear wave theory, provides the additional component of the bottom shear stress, $\tau_w$, induced by the wind-wave field. The nonlinear interactions between $\tau_w$ and the current-induced bottom shear stress ($\tau_t$) are accounted for by means of the empirical formulation by Soulsby (*56*), which increases the value of the total bottom shear stress, $\tau_b$, beyond the mere sum of $\tau_t$ and $\tau_w$.

Using the same computational grid, the STABEM module (*29*) solves the advection-diffusion equation for suspended sediment with a conservative, second-order in-space scheme and the Exner's equation

$$\frac{\partial C_i Y}{\partial t} + \nabla \cdot (\boldsymbol{q}\, C_i) - \nabla \cdot (\mathbf{D}_h \nabla C_i) = E_i - D_i \quad i = s, m \tag{6}$$

$$(1-n)\frac{\partial z_b}{\partial t} = \sum_i (D_i - E_i) \tag{7}$$

where $C$ is the depth-averaged sediment concentration; $\mathbf{D}_h(x, y, t)$ is space- and time-dependent 2D diffusivity tensor, assumed equal to the eddy viscosity computed by the hydrodynamic module (*57*); $E$ and $D$ represent the entrainment and deposition of bed sediment; $z_b$ is the bed elevation; and $n$ is the bed porosity, assumed equal to 0.4. The subscript $i$ refers to the noncohesive [sand ($s$)] and cohesive [mud ($m$)] sediment classes that typically characterize the bed of tidal lagoons. The relative content of mud ($p_m$), which represents the sum of clay and silt, is assumed to vary both in time and space; it determines the cohesive or noncohesive behavior of the mixture and the critical value of the bottom shear stress. The threshold value of mud content $p_{mc} = 10\%$ is assumed to discriminate between noncohesive and cohesive behaviors (*58*). On the basis of measurements in the Venice Lagoon, the median diameters $D_{50}$ adopted in the simulations to describe cohesive and noncohesive sediments are 20 and 200 μm, respectively (*29*).

The deposition rate of sand $D_s$ is computed as

$$D_s = w_s r_0 C_s \tag{8}$$

where $w_s$ is the absolute value of the sand settling velocity, and $r_0$ is the ratio of near-bed to depth-averaged concentration, which is here assumed constant and equal to 1.4 (*59*).

The deposition rate of pure cohesive mud, $D_m$, is given by Krone's formula

$$D_m = w_m C_m \max\{0; 1 - \tau_b/\tau_d\} \tag{9}$$

where $w_m$ is the absolute value of the mud settling velocity, $\tau_b$ is the bottom shear stress computed by the hydrodynamic module, and $\tau_d$ is the critical shear stress for deposition ($\tau_d = 1.0\ Pa$). The settling velocities, $w_s$ and $w_m$, are computed using the Van Rijn formulation (*60*) for solitary particles in clear and still water, thus not incorporating flocculation effects that are negligible for particle diameter larger than 20 μm (*61*).

The erosion rate strongly depends on the degree of cohesion of the mixture. For noncohesive mixtures ($p_m < p_{mc}$), the erosion rate of sand, $E_s$, is described by the Van Rijn formulation (*60*), whereas the erosion rate of mud, $E_m$, can be computed through the formulation proposed by Van Ledden (*58*) as follows

$$\begin{aligned} E_s &= (1-p_m)\, w_s \cdot 1.5 \left(\frac{D_{50}/Y}{D_*^{0.3}}\right) T^{1.5} \\ E_m &= \frac{p_m}{1-p_m} M_{nc}\, T \end{aligned} \quad \text{for } p_m < p_{mc} \tag{10}$$

For cohesive mixtures ($p_m > p_{mc}$), both sand and mud erosion rates can be computed using the Partheniades' formula

$$\begin{aligned} E_s &= (1-p_m) \cdot M_c\, T \\ E_m &= p_m \cdot M_c\, T \end{aligned} \quad \text{for } p_m > p_{mc} \tag{11}$$

In Eqs. 10 and 11, $D^*$ is the dimensionless grain size {$D^* = D_{50}[(s-1)g/\nu^2]^{1/3}$, $s$ being the sediment-specific density and ν the water kinematic viscosity}, $T$ is the transport parameter, $M_{nc}$ and $M_c$ are the specific entrainment for noncohesive and cohesive mixtures, respectively (*58*, *60*)

$$M_{nc} = \alpha \frac{\sqrt{(s-1)\, g D_{50}}}{D_*^{0.9}}, M_c = \left(\frac{M_{nc}}{M_m} \cdot \frac{1}{1-p_{mc}}\right)^{\frac{1-p_m}{1-p_{mc}}} \cdot M_m \tag{12}$$

where $M_m$ is the specific entrainment for pure mud ($M_m = 5 \cdot 10^{-2}$ g m/s), and α is set equal to $1 \cdot 10^{-5}$.

The transport parameter is usually defined as $T = \max\{0; \tau_b/\tau_c - 1\}$, describing a sharp transition between $T = 0$ and $T = \tau_b/\tau_c - 1$, where $\tau_b$ is the local bottom shear stress and $\tau_c$ is the critical shear stress for erosion. However, in real tidal systems, both $\tau_b$ and $\tau_c$ are not constant in space; thus, we assume that they are both random variables following a log-normal distribution (*29*). The result of this stochastic approach is a smooth transition between $T = 0$ and $T = \tau_b/\tau_c - 1$.

All parameters are within the range of variability of similar deposition and erosion formulations (*62*, *63*). In particular, erosion is set equal to zero on salt marshes because vegetation reduces velocity and dampens waves, protecting sediment from erosion (*21*, *62*).

The result of erosion and deposition fluxes of sand and mud is a variation in bed level through time, which is computed according to Eq. 7.

The model has been widely benchmarked against hydrodynamic, wind-wave, and turbidity field and satellite data from the Venice Lagoon (Italy) (*30*, *36*), Virginia Coast Reserve lagoons (United States) (*64*), and Cadiz Bay (Spain) (*65*).

The computational domain representing the Venice Lagoon (fig. S1) consists of 51,084 nodes and 96,751 triangular elements. The model is forced with water levels measured at the three inlets as well as with wind directions and velocities measured in three different zones of the lagoon by the Venice Municipality "Centro Previsioni e Segnalazioni Maree" monitoring network (fig. S1). The 3 October event simulation starts 80 hours before closure of the floodgates and ends 32 hours after barrier opening. The 15 October event simulation starts 54 hours before closure of the floodgates and ends 59 hours after the subsequent opening. Moreover, to evaluate the effects of the barrier closures on the sediment budget at a seasonal time scale, we simulated the whole period between 30 September 2020 and 10 January 2021 to cover all the first 15 barrier operations.

Last, a Lagrangian particle tracking scheme has been set up to visualize the fate of sediments that are suspended at a given location

and time instant (see Fig. 6), according to the actual sediment dynamics computed by the Eulerian scheme implemented in STABEM. We release a large number of noninertial particles at a given location and move them according to the velocity field computed by the hydrodynamic module adding a stochastic component, with the local eddy viscosity to measure the diffusivity, to simulate a random walk process (*66*). To account for deposition, at each time step and for each cell of the mesh, we compute the number of particles within the cell, $n_j$, and the ratio of deposited to the total suspended material, $R_D = dt \cdot D/(CY)$, with $dt$ as the time step, and $D$ and $C$ as the total (sand plus mud) deposition rate and vertically averaged concentration, respectively. Given that $R_D$ expresses the probability of deposition of suspended particles in the cell according to STABEM computations, in the Lagrangian particle tracking scheme, $n_{stop} = R_D \cdot n_j$ particles are permanently stopped at each time step. To account for the fractional part of $n_{stop}$, denoted as frac($n_{stop}$), we generate a random number $r \in [0,1]$ and stop an additional particle if $r <$ frac($n_{stop}$). The number of released particles, $N_p = 10{,}000$, is large enough to make the percentages of particles deposited on the marsh (Fig. 6) independent of $N_p$.

## SUPPLEMENTARY MATERIALS

Supplementary material for this article is available at https://science.org/doi/10.1126/sciadv.abm8446

## REFERENCES AND NOTES


1. R. J. Nicholls, P. P. Wong, V. Burkett, J. O. Codignotto, J. E. Hay, R. F. McLean, S. Ragoonaden, C. D. Woodroffe, in *Climate Change 2007: Impacts, Adaptation and Vulnerability. Contribution of Working Group II to the Fourth Assessment Report of the Intergovernmental Panel on Climate Change*, M. L. Parry, O. F. Canziani, J. P. Palutikof, P. J. van der Linden, C. E. Hanson, Eds. (Cambridge Univ. Press, 2007), pp. 315–356.
2. E. Kirezci, I. R. Young, R. Ranasinghe, S. Muis, R. J. Nicholls, D. Lincke, J. Hinkel, Projections of global-scale extreme sea levels and resulting episodic coastal flooding over the 21st Century. *Sci. Rep.* **10**, 1–12 (2020).
3. R. J. Nicholls, D. Lincke, J. Hinkel, S. Brown, A. T. Vafeidis, B. Meyssignac, S. E. Hanson, J.-L. Merkens, J. Fang, A global analysis of subsidence, relative sea-level change and coastal flood exposure. *Nat. Clim. Chang.* **11**, 338–342 (2021).
4. M. Oppenheimer, B. C. Glavovic, J. Hinkel, R. van de Wal, A. K. Magnan, A. Abd-Elgawad, R. Cai, M. Cifuentes-Jara, R. M. DeConto, T. Ghosh, J. Hay, F. Isla, B. Marzeion, B. Meyssignac, Z. Sebesvari, Sea level rise and implications for low-lying islands, coast and communitites, in *Intergovernmental Panel on Climate Change (IPCC) Special Report on the Ocean and Cryosphere in a Changing Climate*. H. O. Portner, D. C. Roberts, V. Masson-Delmotte, P. Zhai, M. Tignor, E. Poloczanska, K. Mintenbeck, A. Alegria, M. Nicolai, A. Okem, J. Petzold, B. Rama, N. M. Weyer, eds. (Cambridge Univ. Press, Cambridge, UK, 2019). pp. 321–445.
5. M. I. Vousdoukas, L. Mentaschi, J. Hinkel, P. J. Ward, I. Mongelli, J.-C. Ciscar, L. Feyen, Economic motivation for raising coastal flood defenses in Europe. *Nat. Commun.* **11**, 2119 (2020).
6. L. F. Mooyaart, S. N. Jonkman, Overview and design considerations of storm surge barriers. *J. Waterw. Port, Coastal, Ocean Eng.* **143**, 06017001 (2017).
7. M. Eelkema, Z. B. Wang, A. Hibma, M. J. F. Stive, Morphological effects of the eastern scheldt storm surge barrier on the ebb-tidal delta. *Coast. Eng. J.* **55**, 1350010–1350026 (2013).
8. P. Orton, S. Fernald, K. Marcell, B. Brooks, B. Van Prooijen, Z. Chen, Surge Barrier Environmental Effects and Empirical Experience Workshop Report 31 p. Available at: https://philiporton.com/2018/11/04/storm-surge-barriers-and-the-hudson-river-estuary/ (2019).
9. Z. Zhou, G. Coco, I. Townend, M. Olabarrieta, M. van der Wegen, Z. Gong, A. D'Alpaos, S. Gao, B. E. Jaffe, G. Gelfenbaum, Q. He, Y. Wang, S. Lanzoni, Z. B. Wang, H. Winterwerp, C. Zhang, Is "Morphodynamic Equilibrium" an oxymoron? *Earth-Science Rev.* **165**, 257–267 (2017).
10. T. de Haas, H. J. Pierik, A. J. F. F. van der Spek, K. M. Cohen, B. van Maanen, M. G. Kleinhans, Holocene evolution of tidal systems in The Netherlands: Effects of rivers, coastal boundary conditions, eco-engineering species, inherited relief and human interference. *Earth-Science Rev.* **177**, 139–163 (2018).
11. M. O. Green, G. Coco, Review of wave-driven sediment resuspension and transport in estuaries. *Rev. Geophys.* **52**, 77–117 (2014).
12. J. F. Rodríguez, P. M. Saco, S. G. Sandi, N. Saintilan, G. Riccardi, Potential increase in coastal wetland vulnerability to sea-level rise suggested by considering hydrodynamic attenuation effects. *Nat. Commun.* **8**, 16094 (2017).
13. D. M. Peteet, J. Nichols, T. Kenna, C. Chang, J. Browne, M. Reza, S. Kovari, L. Liberman, S. Stern-Protz, Sediment starvation destroys New York City marshes' resistance to sea level rise. *Proc. Natl. Acad. Sci. U.S.A.* **115**, 10281–10286 (2018).
14. R. A. Mel, D. Pietro Viero, L. Carniello, A. Defina, L. D'Alpaos, The first operations of Mo.S.E. system to prevent the flooding of Venice: Insights on the hydrodynamics of a regulated lagoon. *Estuar. Coast. Shelf Sci.* **261**, 107547 (2021).
15. A. J. Ammerman, C. E. McClennen, Saving venice. *Science* **289**, 1301–1302 (2000).
16. R. L. Bras, D. R. F. Harleman, A. Rinaldo, P. Rizzoli, Rescuing venice from a watery grave. *Science* **291**, 2315–2316 (2001).
17. D. G. Aubrey, P. E. Speer, A study of non-linear tidal propagation in shallow inlet/estuarine systems Part I: Observations. *Estuar. Coast. Shelf Sci.* **21**, 185–205 (1985).
18. I. Möller, M. Kudella, F. Rupprecht, T. Spencer, M. Paul, B. K. van Wesenbeeck, G. Wolters, K. Jensen, T. J. Bouma, M. Miranda-Lange, S. Schimmels, Wave attenuation over coastal salt marshes under storm surge conditions. *Nat. Geosci.* **7**, 727–731 (2014).
19. G. Mariotti, S. Fagherazzi, Wind waves on a mudflat: The influence of fetch and depth on bed shear stresses. *Cont. Shelf Res.* **60**, S99–S110 (2013).
20. L. Tommasini, L. Carniello, M. Ghinassi, M. Roner, A. D'Alpaos, Changes in the wind-wave field and related salt-marsh lateral erosion: Inferences from the evolution of the Venice Lagoon in the last four centuries. *Earth Surf. Process. Landforms.* **44**, 1633–1646 (2019).
21. I. Möller, T. Spencer, J. R. French, D. J. Leggett, M. Dixon, Wave transformation over salt marshes: A field and numerical modelling study from north Norfolk. *England. Estuar. Coast. Shelf Sci.* **48**, 411–426 (1999).
22. S. Silvestri, A. D'Alpaos, G. Nordio, L. Carniello, Anthropogenic modifications can significantly influence the local mean sea level and affect the survival of salt marshes in shallow tidal systems. *J. Geophys. Res. Earth Surf.* **123**, 996–1012 (2018).
23. R. Costanza, R. d'Arge, R. de Groot, S. C. Farber, M. Grasso, B. Hannon, K. Limburg, S. Naeem, R. V. O'Neill, J. Paruelo, R. G. Raskin, P. Sutton, M. van den Belt, The value of the world's ecosystem services and natural capital. *Nature* **387**, 253–260 (1997).
24. G. L. Chmura, S. C. Anisfeld, D. R. Cahoon, J. C. Lynch, Global carbon sequestration in tidal, saline wetland soils. *Global Biogeochem. Cycles* **17**, 1111 (2003).
25. E. B. Barbier, S. D. Hacker, C. Kennedy, E. W. Koch, A. C. Stier, B. R. Silliman, The value of estuarine and coastal ecosystem services. *Ecol. Monogr.* **81**, 169–193 (2011).
26. A. Newton, A. C. Brito, J. D. Icely, V. Derolez, I. Clara, S. Angus, G. Schernewski, M. Inácio, A. I. Lillebø, A. I. Sousa, B. Béjaoui, C. Solidoro, M. Tosic, M. Cañedo-Argüelles, M. Yamamuro, S. Reizopoulou, H.-C. Tseng, D. M. Canu, L. Roselli, M. Maanan, S. Cristina, A. C. Ruiz-Fernández, R. F. de Lima, B. Kjerfve, N. Rubio-Cisneros, A. Pérez-Ruzafa, C. Marcos, R. Pastres, F. Pranovi, M. Snoussi, J. Turpie, Y. Tuchkovenko, B. Dyack, J. Brookes, R. Povilanskas, V. Khokhlov, Assessing, quantifying and valuing the ecosystem services of coastal lagoons. *J. Nat. Conserv.* **44**, 50–65 (2018).
27. R. L. Bras, D. R. F. Harleman, A. Rinaldo, P. Rizzoli, [Reply to "Did the Italian Government approve an obsolete project to save Venice?" by P.A. Pirazzoli] Obsolete? No. Necessary? Yes. The gates will save Venice. *Eos, Trans. Am. Geophys. Union.* **83**, 217 (2002).
28. R. A. Mel, L. Carniello, L. D'Alpaos, How long the Mo.S.E. barriers will be effective in protecting all the urban settlements in the Venice lagoon? The wind setup constraint. *Coast. Eng.* **168**, 103923 (2021).
29. L. Carniello, A. Defina, L. D'Alpaos, L. D'Alpaos, Modeling sand-mud transport induced by tidal currents and wind waves in shallow microtidal basins: Application to the Venice Lagoon (Italy). *Estuar. Coast. Shelf Sci.* **102-103**, 105–115 (2012).
30. L. Carniello, A. D'Alpaos, A. Defina, Modeling wind waves and tidal flows in shallow micro-tidal basins. *Estuar. Coast. Shelf Sci.* **92**, 263–276 (2011).
31. C. Ferrarin, A. Tomasin, M. Bajo, A. Petrizzo, G. Umgiesser, Tidal changes in a heavily modified coastal wetland. *Cont. Shelf Res.* **101**, 22–33 (2015).
32. L. Carniello, A. Defina, L. D'Alpaos, Morphological evolution of the Venice lagoon: Evidence from the past and trend for the future. *J. Geophys. Res. Earth Surf.* **114**, F04002 (2009).
33. S. Fagherazzi, L. Carniello, L. D'Alpaos, A. Defina, Critical bifurcation of shallow microtidal landforms in tidal flats and salt marshes. *Proc. Natl. Acad. Sci.* **103**, 8337–8341 (2006).
34. A. Defina, L. Carniello, S. Fagherazzi, L. D'Alpaos, Self-organization of shallow basins in tidal flats and salt marshes. *J. Geophys. Res.* **112**, F03001 (2007).
35. A. D'Alpaos, L. Carniello, A. Rinaldo, Statistical mechanics of wind wave-induced erosion in shallow tidal basins: Inferences from the Venice Lagoon. *Geophys. Res. Lett.* **40**, 3402–3407 (2013).
36. L. Carniello, S. Silvestri, M. Marani, A. D'Alpaos, V. Volpe, A. Defina, Sediment dynamics in shallow tidal basins: In situ observations, satellite retrievals, and numerical modeling in the Venice Lagoon. *J. Geophys. Res. Earth Surf.* **119**, 802–815 (2014).
37. M. Pivato, L. Carniello, I. Moro, P. D'Odorico, On the feedback between water turbidity and microphytobenthos growth in shallow tidal environments. *Earth Surf. Process. Landforms.* **44**, 1192–1206 (2019).
38. A. D'Alpaos, S. M. Mudd, L. Carniello, Dynamic response of marshes to perturbations in suspended sediment concentrations and rates of relative sea level rise. *J. Geophys. Res. Earth Surf.* **116**, 1–13 (2011).

39. M. Marani, A. D'Alpaos, S. Lanzoni, L. Carniello, A. Rinaldo, The importance of being coupled: Stable states and catastrophic shifts in tidal biomorphodynamics. *J. Geophys. Res. Earth Surf.* **115**, 1–15 (2010).
40. J. T. Morris, P. V. Sundareshwar, C. T. Nietch, B. Kjerfve, D. R. Cahoon, Responses of coastal wetlands to rising sea level. *Ecology* **83**, 2869–2877 (2002).
41. M. L. Kirwan, J. P. Megonigal, Tidal wetland stability in the face of human impacts and sea-level rise. *Nature* **504**, 53–60 (2013).
42. D. Tognin, A. D'Alpaos, M. Marani, L. Carniello, Marsh resilience to sea-level rise reduced by storm-surge barriers in the Venice Lagoon. *Nat. Geosci.* **14**, 906–911 (2021).
43. M. Marani, A. D'Alpaos, S. Lanzoni, M. Santalucia, Understanding and predicting wave erosion of marsh edges. *Geophys. Res. Lett.* **38**, 1944–8007 (2011).
44. N. Leonardi, N. K. Ganju, S. Fagherazzi, A linear relationship between wave power and erosion determines salt-marsh resilience to violent storms and hurricanes. *Proc. Natl. Acad. Sci. U.S.A.* **113**, 64–68 (2016).
45. A. Finotello, A. Canestrelli, L. Carniello, M. Ghinassi, A. D'Alpaos, Tidal flow asymmetry and discharge of lateral tributaries drive the evolution of a microtidal meander in the Venice Lagoon (Italy). *J. Geophys. Res. Earth Surf.* **124**, 3043–3066 (2019).
46. A. D'Alpaos, C. Da Lio, M. Marani, Biogeomorphology of tidal landforms: Physical and biological processes shaping the tidal landscape. *Ecohydrology*. **5**, 550–562 (2012).
47. M. J. Baptist, T. Gerkema, B. C. van Prooijen, D. S. van Maren, M. van Regteren, K. Schulz, I. Colosimo, J. Vroom, T. van Kessel, B. Grasmeijer, P. Willemsen, K. Elschot, A. V. de Groot, J. Cleveringa, E. M. M. van Eekelen, F. Schuurman, H. J. de Lange, M. E. B. van Puijenbroek, Beneficial use of dredged sediment to enhance salt marsh development by applying a 'Mud Motor'. *Ecol. Eng.* **127**, 312–323 (2019).
48. S. Temmerman, P. Meire, T. J. Bouma, P. M. J. Herman, T. Ysebaert, H. J. De Vriend, Ecosystem-based coastal defence in the face of global change. *Nature* **504**, 79–83 (2013).
49. S. Temmerman, M. L. Kirwan, Building land with a rising sea. *Science (80-. ).* **349**, 588–589 (2015).
50. M. S. N. Chowdhury, B. Walles, S. Sharifuzzaman, M. Shahadat Hossain, T. Ysebaert, A. C. Smaal, Oyster breakwater reefs promote adjacent mudflat stability and salt marsh growth in a monsoon dominated subtropical coast. *Sci. Rep.* **9**, 8549 (2019).
51. L. Carbognin, P. Teatini, L. Tosi, Eustacy and land subsidence in the Venice Lagoon at the beginning of the new millennium. *J. Mar. Syst.* **51**, 345–353 (2004).
52. A. Defina, Two-dimensional shallow flow equations for partially dry areas. *Water Resour. Res.* **36**, 3251–3264 (2000).
53. J. Smagorinsky, General circulation experiments with the primitive equations: I. The basic experiment. *Mon. Weather Rev.* **91**, 99–164 (1963).
54. L. H. Holthuijsen, N. Booij, T. H. C. Herbers, A prediction model for stationary, short-crested waves in shallow water with ambient currents. *Coast. Eng.* **13**, 23–54 (1989).
55. I. R. Young, L. A. Verhagen, The growth of fetch limited waves in water of finite depth. Part 1. Total energy and peak frequency. *Coast. Eng.* **29**, 47–78 (1996).
56. R. L. Soulsby, in *Advances in Coastal Morphodynamics*, M. J. F. Stive, Ed. (Delft Hydraulics, 1995), pp. 4-20–4-23.
57. D. Pietro Viero, A. Defina, Water age, exposure time, and local flushing time in semi-enclosed, tidal basins with negligible freshwater inflow. *J. Mar. Syst.* **156**, 16–29 (2016).
58. M. van Ledden, Z.-B. Wang, H. Winterwerp, H. de Vriend, Sand-mud morphodynamics in a short tidal basin. *Ocean Dyn.* **54**, 385–391 (2004).
59. G. Parker, M. Garcia, Y. Fukushima, W. Yu, Experiments on turbidity currents over an erodible bed. *J. Hydraul. Res.* **25**, 123–147 (1987).
60. L. C. van Rijn, Sediment transport, part II: Suspended load transport. *J. Hydraul. Eng.* **110**, 1613–1641 (1984).
61. A. J. Mehta, E. J. Hayter, W. R. Parker, R. B. Krone, A. M. Teeter, Cohesive sediment transport. I: Process description. *J. Hydraul. Eng.* **115**, 1076–1093 (1989).
62. S. Temmerman, T. J. Bouma, G. Govers, Z. B. Wang, M. B. De Vries, P. M. J. Herman, Impact of vegetation on flow routing and sedimentation patterns: Three-dimensional modeling for a tidal marsh. *J. Geophys. Res. Earth Surf.* **110**, 19 (2005).
63. A. Breda, P. M. Saco, S. G. Sandi, N. Saintilan, G. Riccardi, J. F. Rodríguez, Accretion, retreat and transgression of coastal wetlands experiencing sea-level rise. *Hydrol. Earth Syst. Sci.* **25**, 769–786 (2021).
64. G. Mariotti, S. Fagherazzi, P. L. Wiberg, K. J. McGlathery, L. Carniello, A. Defina, Influence of storm surges and sea level on shallow tidal basin erosive processes. *J. Geophys. Res.* **115**, C11012 (2010).
65. C. Zarzuelo, A. López-Ruiz, A. D'Alpaos, L. Carniello, M. Ortega-Sánchez, Assessing the morphodynamic response of human-altered tidal embayments. *Geomorphology* **320**, 127–141 (2018).
66. A. W. Visser, Using random walk models to simulate the vertical distribution of particles in a turbulent water column. *Mar. Ecol. Prog. Ser.* **158**, 275–281 (1997).
67. J. I. Allen, P. J. Somerfield, F. J. Gilbert, Quantifying uncertainty in high-resolution coupled hydrodynamic-ecosystem models. *J. Mar. Syst.* **64**, 3–14 (2007).



**Acknowledgments**

**Funding:** This work was supported by the Research Programme Venezia2021, with the contribution of the Provveditorato for the Public Works of Veneto, Trentino Alto Adige, and Friuli Venezia Giulia, provided through the concessionary of State Consorzio Venezia Nuova and coordinated by CORILA (to A.D.A. and M.M.) and by the 2019 University of Padova project (BIRD199419) entitled "Tidal network ontogeny and evolution: A comprehensive approach based on laboratory experiments with ancillary numerical modelling and field measurements" (L.C.). **Author contributions:** D.T., A.F., A.D.A., and L.C. designed the research. D.T. and A.F. performed the research. All the authors analyzed and discussed the data and model results. L.C., D.P.V., R.A.M., M.P., and A.D. developed the software. D.T. prepared the figures with feedbacks from A.F. D.T. and A.F. wrote the first draft of the manuscript, which was subsequently improved by feedbacks from all the authors. **Competing interests:** The authors declare that they have no competing interests. **Data and materials availability:** All data needed to evaluate the conclusions in the paper are present in the paper and/or the Supplementary Materials. Data are also available at http://researchdata.cab.unipd.it/id/eprint/518. Meteorological data for the Venice Lagoon are also freely available at www.comune.venezia.it/content/dati-dalle-stazioni-rilevamento and www.venezia.isprambiente.it/rete-meteo-mareografica.

Submitted 15 October 2021
Accepted 10 February 2022
Published 1 April 2022
10.1126/sciadv.abm8446

ScienceAdvances

# Loss of geomorphic diversity in shallow tidal embayments promoted by storm-surge barriers

Davide TogninAlvise FinotelloAndrea D'AlpaosDaniele P. VieroMattia PivatoRiccardo A. MelAndrea DefinaEnrico BertuzzoMarco MaraniLuca Carniello

*Sci. Adv.*, 8 (13), eabm8446. • DOI: 10.1126/sciadv.abm8446



*Science Advances* (ISSN ) is published by the American Association for the Advancement of Science. 1200 New York Avenue NW, Washington, DC 20005. The title *Science Advances* is a registered trademark of AAAS.